J. Fluid Mech. (1999), *vol.* 388, *pp.* 21–48. Printed in the United Kingdom

Experiments with constrained chimney-plume flows in the system ammonium chloride–water: comparison with the unconstrained case

By SHAN LIU AND ANGUS HELLAWELL

Metallurgical and Materials Engineering Department, Michigan Technological University, Houghton, MI 49931, USA

(Received 30 September 1997 and in revised form 15 December 1998)

Thermo-solutal chimney-plume flows from a solidifying dendritic mushy region have been promoted in thin-walled glass tubes of internal radii from 0.3 mm–2.0 mm. Flow rates, liquid compositions and temperatures were measured as functions of the depth of immersion of capillary tubes in the advancing mushy region. The results demonstrate competition between buoyancy pressures and the restrictions of liquid recirculation within the dendritic array and have been analysed to provide permeability data for the mushy region at high liquid fractions. These data have been used to make some assessments of channel/plume dimensions for naturally occurring, unconstrained flows in the same system.

1. Introduction

This work is concerned with the chimney or plume flows which rise from channels in a dendritic mushy region, being driven by thermosolutal convection. The situation concerns the escape of buoyant, solutally enriched, cooler liquid from within a dendritic array into warmer, overlying, open liquid, which is solutally of lower concentration and initially quiescent. The natural convection which this density inversion promotes takes place in two stages: initially, within minutes of the development of a dendritic growth front, when the mushy region is only a few mm deep, short range (< 10 mm) convective fingers develop ahead of the front on a lateral scale comparable to that of the primary dendritic spacings (< 0.5 mm); these are oscillatory and irregular in form and location. At a longer time ($\approx$ 20–40 min) one or more of the fingers reinforce and develop into wider (≈ 1 mm) longer range (> 100 mm) chimney patterns with quasi-steady state flows upwards and concomitant reentrainment of the bulk liquid through the mush into the channels which rapidly open below the plumes.

This form of convection has been studied experimentally in some detail, particularly using aqueous salt systems to observe the phenomena directly (e.g. McDonald & Hunt 1969, 1970; Copley *et al.* 1970; Sample & Hellawell 1982, 1984; Bennon & Incropera 1987; Chen & Chen 1991; Tait & Jaupart 1992; Chen 1995). It has also been studied in metals on a laboratory scale (e.g. Sarazin & Hellawell 1988; Bergman *et al.* 1997) and is a widely recognized defect in metallurgical castings where the chimney-channels appear as residual chains of polycrystalline, solute enhanced material, termed 'A' segregates in steel ingots (e.g. Moore & Shah 1983) or 'freckles' in directionally solidified castings (e.g. Copley *et al.* 1970). The phenomena are also of geological and oceanographic significance and have been widely discussed in the literature. A number of reviews by Worster (1991, 1997) contain much of this published material

and discussion of the theoretical basis for the initiation and propagation of channel-chimney flows.

What is of particular concern here is that the scale of these chimney-channel patterns, developed under laboratory conditions, is very similar in different material systems, including organics (Hellawell, Sarazin & Steube 1993). Thus, in metals, aqueous salts and organics, covering a range of Prandtl numbers of some three orders of magnitude, channels are always around 0.5 mm to 1.0 mm in radius, spaced some 5 mm to 10 mm apart, although the flow rates differ considerably from about $1\,\mathrm{mm\,s^{-1}}$ in organics, to $\approx 10\,\mathrm{mm\,s^{-1}}$ in aqueous systems, to an estimated order of up to $\approx 100\,\mathrm{mm\,s^{-1}}$ in metals. Of the relevant physical properties, only the dynamic viscosities, η, are similar, lying between 1.10^{-3} and $2.5 \times 10^{-3}\ \mathrm{kg\,m^{-1}\,s^{-1}}$ (Pa s).

The nearly steady-state flow rates and dimensions (widths and spacings) which are characteristic of unconstrained established channels and chimney plumes are selected by a compromise between the buoyancy attending density inversion and the restrictions to entrainment of bulk liquid around and below a channel mouth. It was the object of the present work to observe how a system would respond to constrained channels within tubes of predetermined widths. To this end, experiments have been conducted with the aqueous ammonium chloride system, in which chimney-plume convection was promoted within thin-walled glass tubes of different radii across a range including that typical of unconstrained examples. While there are some obvious differences between the constrained and unconstrained situations the experimental results have provided an interesting assessment of the opposing contributions of buoyancy and entrainment limitations, sufficient to provide some useful estimates of the permeability of the mushy region in this aqueous system. These results have then been used to make some predictions about the dimensions of unconstrained, naturally occurring channel/chimney plumes.

2. Experimental

Experiments were carried out with a solution of NH_4Cl–70 wt%H_2O (see phase diagram, figure 1). For the purposes of this study, NH_4Cl is the primary solid phase and H_2O is the less dense solute component which accumulates in the liquid as solidification takes place. This notation is followed in order to be consistent with the general case of systems in which thermosolutal convection may occur.

Referring to figure 1 for a composition of 70 wt%H_2O, it can be seen that the equilibrium liquid fraction, f_L, falls from unity at the liquidus, at 35 °C, to ≈ 0.86 by weight at the eutectic temperature of −16 °C. With adjustments for densities ($\rho\,NH_4Cl = 1530\,\mathrm{kg\,m^{-3}}$ and ρ liquid $\approx 1080\,\mathrm{kg\,m^{-3}}$), this translates to a volume fraction of ≈ 0.9, or solid volume fraction, $f_S = 1 - f_L \approx 0.1$. In practice, with macrosegregation during solidification, the solid fraction actually approaches 0.15 at the eutectic temperature (Hellawell *et al.* 1993), but the mushy region is very porous (see § 4 and Appendix E).

The solution was poured at 75 °C into a transparent Perspex container or mould, cooled from below by a copper block which was connected to a liquid nitrogen pump. The mould dimensions were height = 200 mm, width = 45 mm and depth = 6 mm deep, and the contents were viewed through an optical microscope using various illumination modes, as described in Steube & Hellawell 1993. The cell could be viewed directly or be photographed, but events were always followed and recorded by a video camera at 30 frames/s for the duration of an experiment. We note that the mould depth or thickness (6 mm) was somewhat less than the typical spacing of naturally

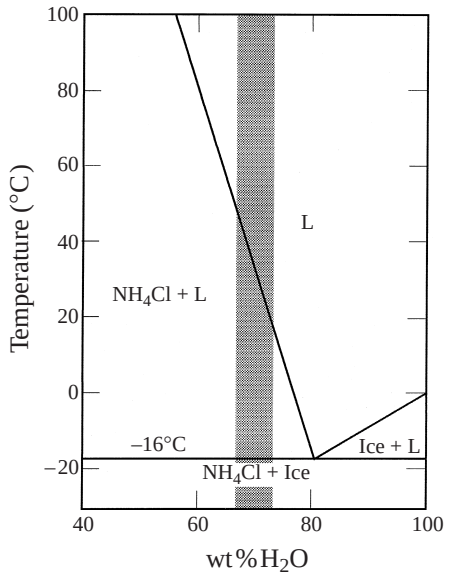

FIGURE 1. Partial phase diagram for the system NH_4Cl-H_2O.

occurring, unconstrained channels ($L \approx 5$–10 mm), so that in these experiments the entrainment area was also partly constrained towards a two-dimensional configuration by the mould walls–this is considered later, see Appendix F.

Glass tubes containing water, closed at the top, were preset in position within the bulk liquid at such a height that the dendritic front approached the lower ends after about 40 min. At this time, the dendritic and eutectic fronts were separated by a mushy region about 13 mm deep and natural channel development was imminent. The tubes and their contents were in local thermal equilibrium with the open bulk liquid. Chimney-plume convection within the tubes was then promoted by opening the tops and allowing the water prime to escape. Figure 2 shows the arrangement schematically, and figure 3 corresponds to detail at a later time when the growth front had advanced so that the base of the tube was immersed within the mushy region to a depth, d. Other relevant dimensions are as shown.

The tube wall thicknesses were 0.1 mm. Tubes were typically 60 mm long, although experiments were also performed with longer and shorter tubes. Tube internal radii were 0.4, 0.5 and 0.75 mm, with some qualitative observations of flow in wider tubes up to 2 mm radius and narrower tubes of radii 0.3 and 0.25 mm.

The duration of the experiments was determined by the time taken for the eutectic front to grow up to the base of a tube, when it became closed and convection ceased. The dendritic and eutectic fronts advance at rates which decrease parabolically (e.g. Jang & Hellawell 1991). All experiments began at approximately the same time after pouring when the mushy region was 13 ± 1 mm deep and ended after 2200 s (35 min) when the eutectic front reached the base of a tube. At the end of an experiment the mushy region was around 23 mm deep because the dendritic front advances more rapidly. Experimental results were therefore expressed as functions of the depth d, as a fraction of the mushy zone depth, h, at any given time (see figure 3). The positions of the growth fronts and the duration of an experiment can be understood from figure 4: the dendritic front advances 23 mm in 2100 s, or with a mean growth rate of $10\,\mu m\,s^{-1}$.

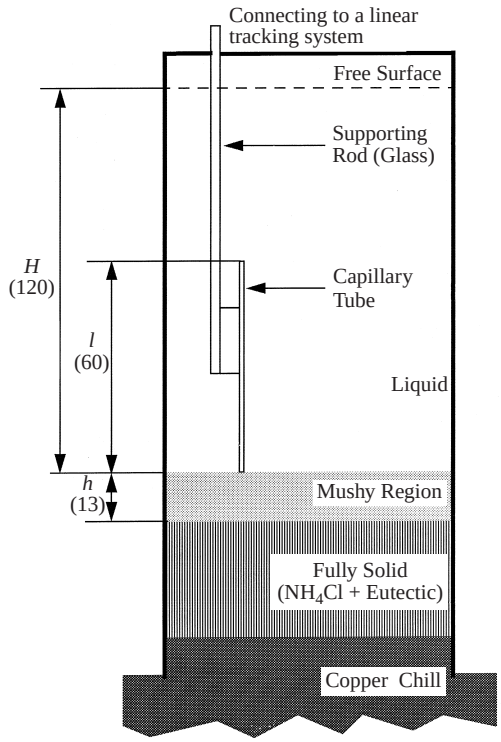

FIGURE 2. Experimental arrangement when the dendritic front has reached the base of a capillary tube. The numbers in brackets are in mm.

During this time interval, the liquid was sampled within the tubes and in the bulk liquid near the top of tubes using a fine micropipette. This liquid was immediately transferred to a Pulfricht-type refractometer and the composition was determined from the refractive index, calibrated with respect to NH_4Cl content and temperature. Compositions were reproducible to within ± 0.1 wt % (see Sarazin 1990; Hellawell *et al.* 1993).

At the same times, temperatures were measured for the plume liquid escaping from the top of tubes and the adjacent bulk liquid, using a fine (0.25 mm) chromel–alumel thermocouple. The temperatures at the bases of tubes were also recorded in the same way, corresponding to that of liquid entrained. Occasional samplings of compositions and temperatures were also made at positions close to the dendritic growth front and up to the free surface.

Some eight measurements were made for each run and simultaneously the flow velocities within the tubes were recorded from the movement of entrained dendrite fragments, recorded from the video-camera. Such particles were typically less than 50 μm wide, and although more dense than the liquid, even assuming them to be spherical (which they rarely were) Stokes' equation would predict only a small correction of $< 0.5\,\mathrm{mm\,s^{-1}}$ below that of the true fluid flow rate. With measured flow rates of up to $10\,\mathrm{mm\,s^{-1}}$ this correction was overlooked. Only the maximum velocities in the centre of tubes were selected. Synchronization of all these observations and measurements employed two people, well coordinated.

Table 1 includes some physical data and experimental dimensions relevant to the results and their manipulation.

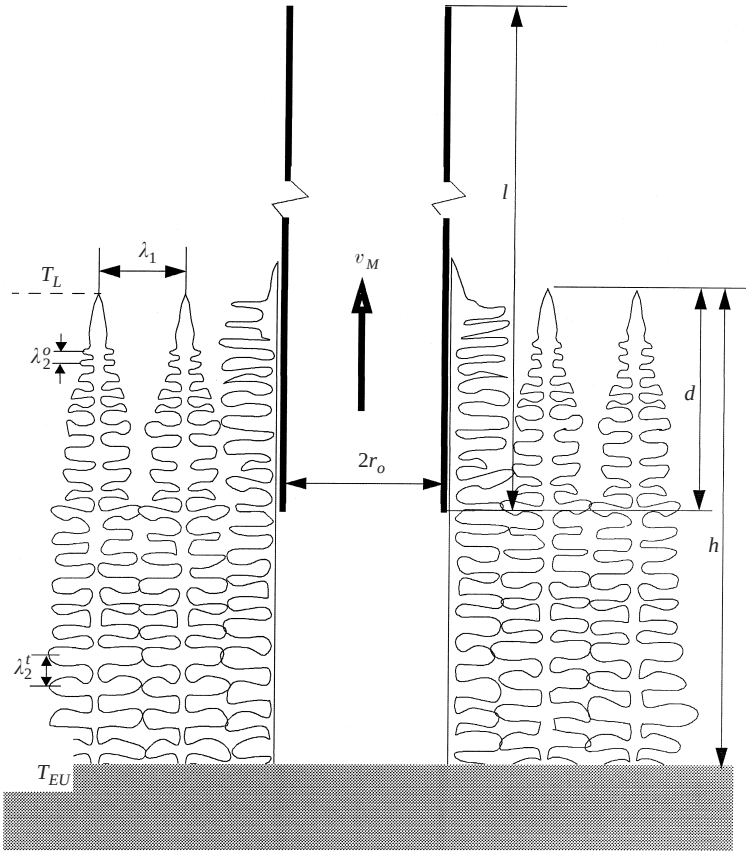

FIGURE 3. Schematic detail around a tube intake after the formation of an open channel with the growth front having advanced a distance d. Other relevant dimensions are as indicated.

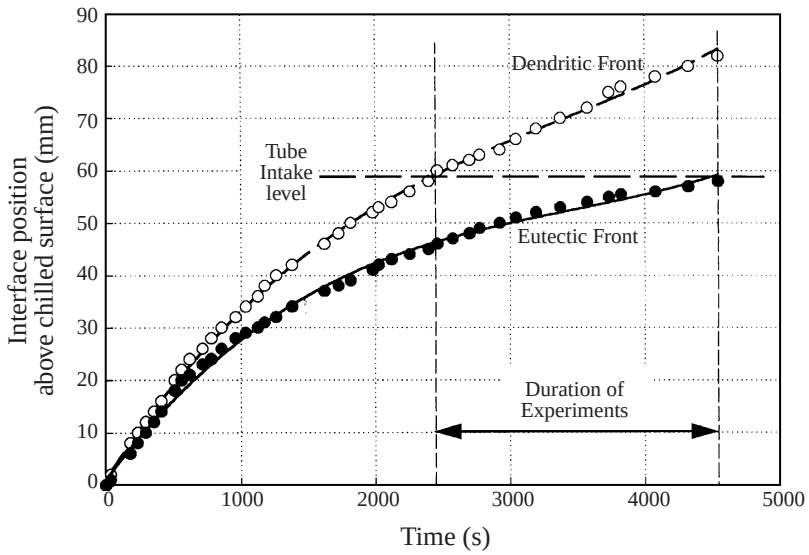

FIGURE 4. Heights of dendritic and eutectic growth fronts *vs.* time. An experiment began when the dendritic front reached a tube base and ended when it became closed by the solid eutectic front after ≈ 2100 s.

NH_4Cl-H_2O liquidus slope, $dT/dc = -4.8$ K wt%$^{-1}$
Liquidus at $C_0 = 70$ wt%$H_2O = 35\,^{\circ}$C
Density, ρ_L at 70 wt%H_2O, 35 °C = 1080 kg m^{-3}
Volume thermal expansion coefficient $\alpha = 3 \times 10^{-4}$ K^{-1}
Volume solutal expansion coefficient $\beta = 2.5 \times 10^{-3}$ wt%$^{-1}$
Thermal diffusivity of liquid, $\kappa_L = 1.47 \times 10^{-7}$ m^2 s^{-1}
Solutal diffusivity of liquid, $D_L = 1.3 \times 10^{-9}$ m^2 s^{-1}
Dynamic viscosity $\eta = 1.03 \times 10^{-3}$ kg m^{-1} s^{-1}
Kinematic viscosity, $\nu = \eta/\rho = 9.54 \times 10^{-7}$ m^2 s^{-1}
Prandtl number, $\nu/\kappa_L = 6.8$
Lewis number, $\kappa_L/D_L = 1.07 \times 10^2$

TABLE 1. Relevant physical and systems data.

3. Results

3.1. *General observations*

As solid grew up from the base of the mould, the temperature of the supernatant bulk liquid fell and it also became enriched in the solute, water, as macroscopic segregation occurred. These trends are illustrated in figure 5. As the water content rose, the temperature at the dendritic growth front fell accordingly, as shown. Measurements attending tube flow typically began after about 35 min when the bulk liquid was mixed mainly by shorter-range finger convection and the vertical water concentration gradient was slightly negative. With the onset of longer-range convection the bulk liquid became increasingly water rich at higher levels. The duration of a run corresponded in figure 5 to times after pouring from $>$ 35 min to about 70 min, and during this period the bulk liquid composition rose by about 1 wt %H_2O at the growth front and 2 wt%H_2O at the meniscus.

It should be understood that the release of priming water from the glass tubes was always followed by a surge of activity as interdendritic liquid was drawn upwards, with the simultaneous formation of a channel in the mushy region below and the ejection of large dendritic fragements. The flow then settled down to quasi-steady state after some 5 min as the dendritic front grew around the base of a tube. The glass tubes were not inserted into the mushy region mechanically, but rather the growth front advanced slowly around them. Thus, there was no disturbance to the array other than that attending the initial surge of activity immediately below a tube entrance as a channel opened down to the eutectic front with approximately the same diameter as that of the tube. In this respect, the opening up of a channel in the mushy region, extending down towards the eutectic front, was little different to that occurring for the unconstrained case (see, e.g. Sample & Hellawell 1982). Measurements of flow rates, v_M, liquid compositions and temperatures then commenced as soon as this steady condition became established and continued to the time when the base of a tube was closed by the solid eutectic front–typically about 35 min cf. § 2 and figure 4.

Meanwhile, at the tops of tubes, plume flows accelerated and narrowed as the liquid escaped from the confines of the tube walls, figure 6. These unconstrained plumes then continued some 60 mm to the upper meniscus, as did any other naturally occurring plumes in moulds of this height (e.g. Hellawell *et al.* 1993). This acceleration occurred because at the effux from a tube, surrounding fluid is drawn up with the buoyant

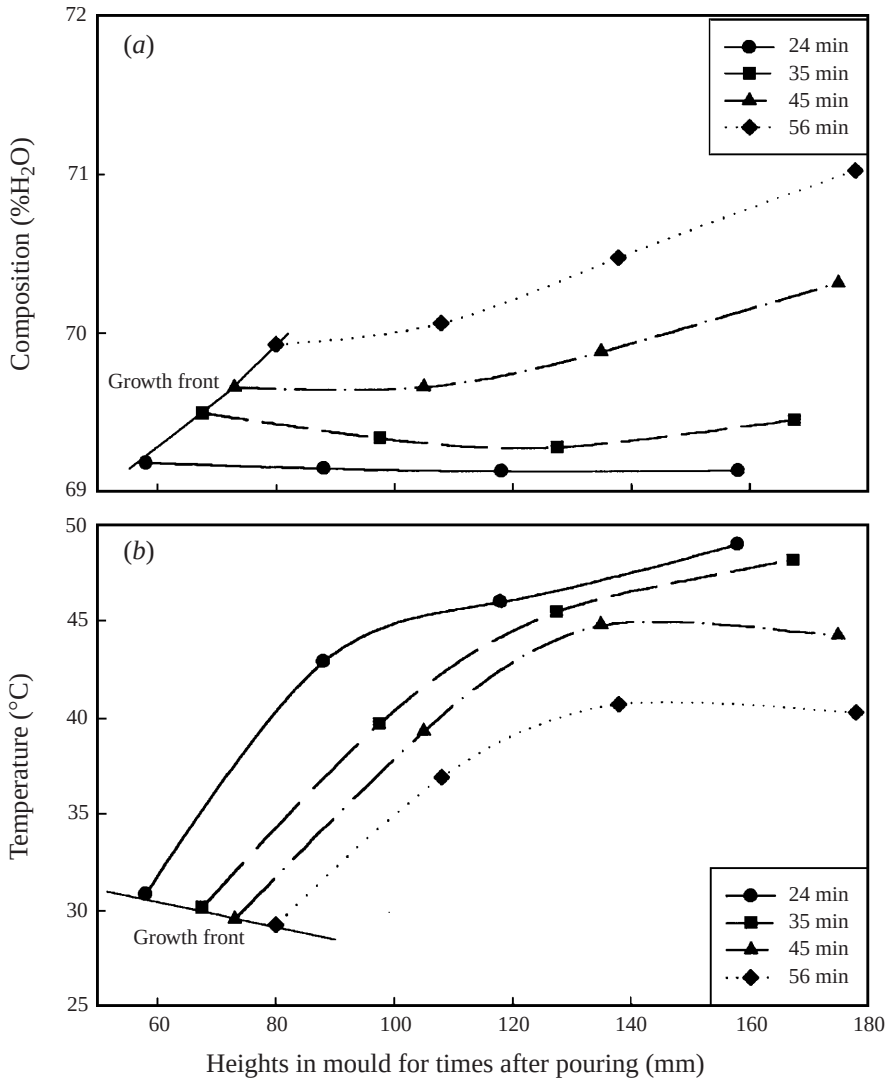

FIGURE 5. (*a*) Composition, and (*b*) temperature measurements in bulk liquid above a growth front after various times. As macrosegregation occurred, the water concentration rose and the temperature at the growth front fell. Experiments began after 40 min and ended after 75 min, cf. figure 4.

plume liquid to give a velocity profile wider than the composition profile which is of step form (hence the sharp step in refractive index). Continuity with this relaxation requires that the product of velocity and cross-sectional area remains constant for the plume core. From figure 6 it may be seen that the width of the unconstrained plume is narrower than the tube bore by $\approx 1 : 3^{1/2}$ and therefore the acceleration was a factor of $\times 3$. An aerodynamic equivalent situation occurs at the efflux of a chimney stack (e.g. Scorer 1978 ch. 8).

Flow at later times became restricted to plumes narrower than the bore of a tube, accompanied by reverse flow into the mouths of tubes from the bulk, Figure 7. The velocity measurements at later stages, when backflow began, relate to that within the plumes which were then narrower than the tube bores. This type of reverse flow

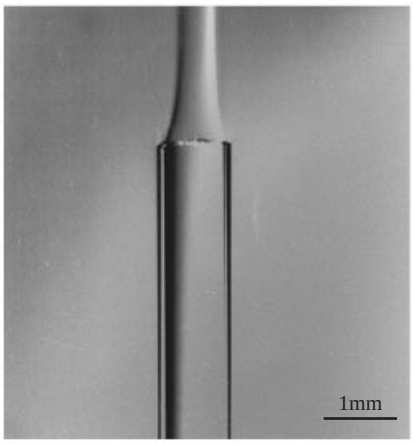

FIGURE 6. Shadowgraph of chimney plume escaping from the top of a tube. The liquid accelerates as it escapes from the constraint of the tube and therefore continuity requires that the unconstrained plume be narrower.

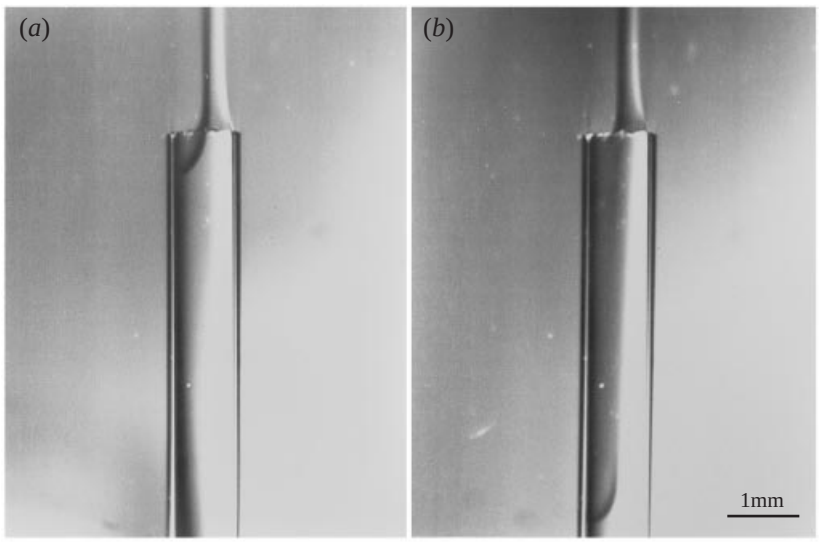

FIGURE 7. Similar to figure 6 but at later stages of an experiment when the lower tube intake became starved by limited entrainment through the mushy region, (*a*) the beginning of reverse inflow and (*b*) some 2 min later.

is similar to 'cold inflow' observed at chimney stack exits when there is insufficient supply of warm gas to sustain streamline flow across the entire diameter (e.g. Jorg & Scorer 1967; Scorer 1978, ch. 10). Once this reverse flow developed, composition measurements within a tube included both internal plume liquid and that entrained downwards from the bulk. This reverse flow did not necessarily persist down to the 'root' of a tube within the mushy region, but its occurrence precluded useful calculations in terms of streamlined flow. Further comment on the onset of this instability is made in § 4 in connection with the pressure terms needed to maintain continuity of flow.

The results of measurements are plotted in figure 8 against the depth of tube immersion, d, expressed as a fraction of the mushy zone depth, h (see figure 3). It should be noted that in all these plots, the individual points are subject to small error bars in velocities ($\approx 0.5\,\mathrm{mm\,s^{-1}}$), in compositions ($\approx 0.2$ wt %) and in positions, d/h (≈ 0.05).

3.2. *Flow rates vs. tube radii*

The variations in flow rates, ■, for three tube radii, $r_0 = 0.4$, 0.5 and 0.75 mm, all of length, $l = 60$ mm, are shown in figure 8. In all cases the velocities passed through maxima which occurred at shorter times (shorter immersions) as the radii increased, falling to zero as tubes were closed by the eutectic front. The maximum speed rose with tube bores from $6\,\mathrm{mm\,s^{-1}}$ to $9\,\mathrm{mm\,s^{-1}}$. The data for times beyond the advent of reverse flow are included in lighter contrast – regime C.

Attempts to promote flow up narrower tubes of 0.25 mm were only partially successful; flow was weak at around $0.2\,\mathrm{mm\,s^{-1}}$ to $0.3\,\mathrm{mm\,s^{-1}}$ and could not be sustained for long times. It may be noted that the primary interdendritic spacing is about the same as the diameter of this narrowest tube and therefore comparable to those of short-range finger patterns.

With wider tubes from 1 mm up to 2 mm radii the flow within a tube was never fully coherent and at 2 mm, the dendritic front actually grew up inside the tube and channels developed internally. The primary dendritic spacing, λ_1 was 0.4 mm to 0.5 mm so that this largest bore corresponded to a diameter of some 8–10 spacings, some three or four times wider than naturally occurring channels.

3.3. *Liquid compositions vs. tube radii*

The corresponding liquid composition differences, ΔC, •, between that in the tubes and that in the surrounding open liquid at the tube exit levels are also plotted in figure 8. These liquid compositions also passed through maxima and then fell abruptly as reverse flow occurred, drawing in bulk liquid containing less water, however, these maxima occurred later in an experimental run (i.e. larger d/h) than the velocity maxima.

For the purpose of subsequent discussion and analysis, these velocity/composition data have been provisionally divided into three regimes; A, when both the compositions and flow rates are rising; B, when the velocities are falling, although the compositions continue to rise; and C, when back inflow occurs and the mean tube liquid compositions also fall. Region C is intractable for useful analysis of buoyancy or streamlined flow and is included only in faint contrast.

It should be remembered that the liquid composition data refer to composition differences between that in tubes and the bulk liquid at the level of tube exits. Also, as noted previously, the bulk liquid compositions rise by 1 wt %H_2O in the course of an experiment, as a result of macrosegregation from chimney transport, constrained and natural, as in figure 5.

3.4. *Temperature measurements*

The temperature changes for a tube of 0.5 mm radius, which are typical and similar to narrower (0.4 mm) and wider (0.75 mm) tubes, are shown in figure 9.

The lower temperatures are those recorded by a thermocouple attached to the base of the tube and are slightly lower than that which would correspond to the liquidus temperature at that level, according to the phase diagram. The plume compositions

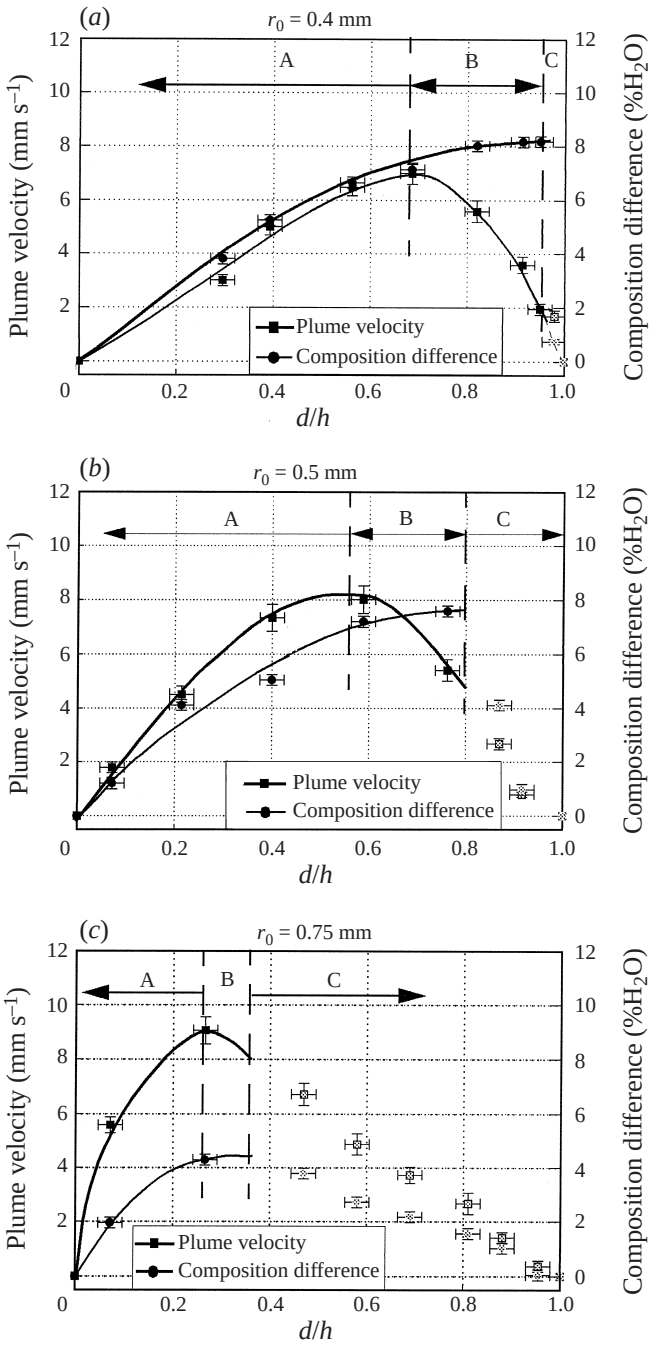

FIGURE 8. Maximum tube flow velocity, v_M, and composition difference, ΔC, between plume liquid and bulk liquid at tube exit, plotted against fractional depth of immersion in the mushy region, d/h, error bars as indicated. Region C corresponds to measurements after reverse inflow occurred. (*a*) $r_0 = 0.4$ mm; (*b*) $r_0 = 0.5$ mm; (*c*) $r_0 = 0.75$ mm.

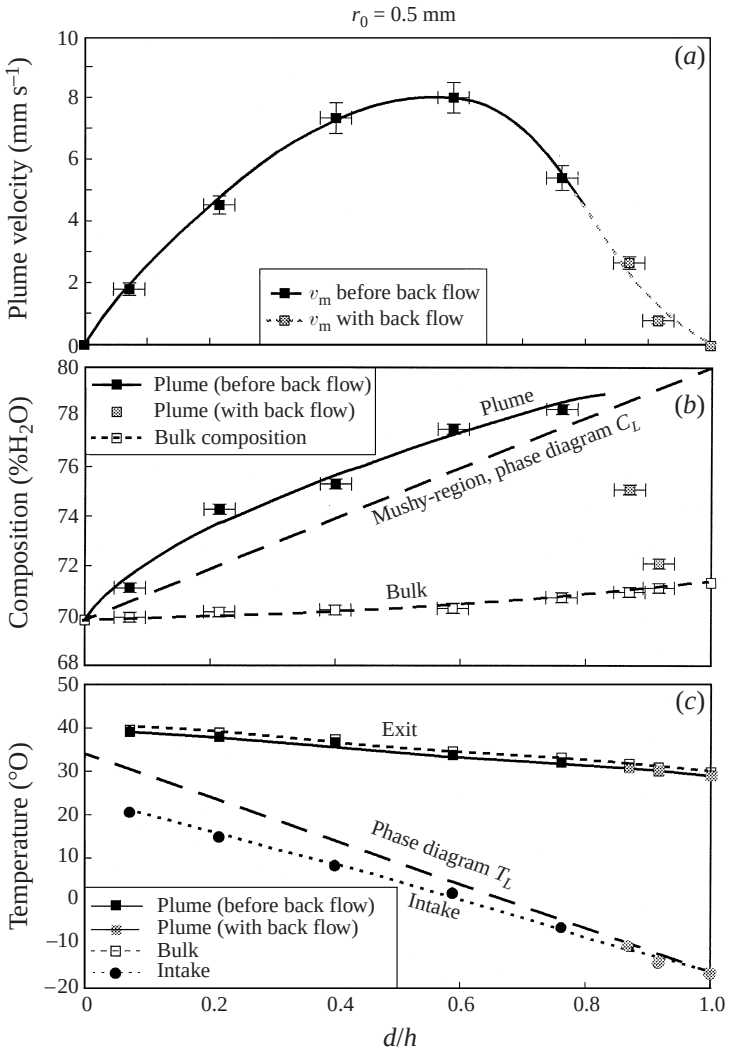

FIGURE 9. Summary of velocity, composition and temperature measurements for tube radius, 0.5 mm, *vs.* fractional depth of immersion in the mushy region, d/h. The compositions, C_L, and temperatures, T_L, are as they would be for a quiescent mushy region.

are also higher. This is because the liquid which is sucked up the tube comes from within a channel at lower levels in the mushy region below the tube intake.

At the tube exit, 60 mm above, the plume liquid has warmed up to within $\approx$ 1 K of the adjacent bulk temperature, i.e. thermal equilibrium was almost, but not quite, achieved as the liquid rose in the tube. This is consistent with observations made on unconstrained, naturally occurring chimney plumes (Hellawell *et al.* 1993), and is in contrast to solutal equilibrium which is not approached to any significant extent, cf. figure 6.

3.5. *Tube length*

In addition to the above, for $l = 60$ mm, flow rates, compositions and temperatures were also recorded with shorter and longer tubes, $l = 30$ mm and $l = 100$ mm for

radius = 0.4 mm. The results for the 60 and 100 mm tubes were very similar and almost within experimental error ranges, those for the shortest tube were only a little lower. Experimental difficulties precluded the sampling of compositions in the shortest tubes, but for those of 60 and 100 mm lengths the differences between escaping plume and bulk liquid compositions were the same within experimental error. Although compositions for the shorter tube are lacking, it may be noted that the tube exit was then relatively close to the dendritic growth front – recollect that with the mushy zone depth of about 23 mm at the end of an experimental run, a 30 mm tube would then project only 7 mm above the front and would therefore, be susceptible to composition fluctuations within the convective finger region. It was concluded, therefore, that tube flow rates were not a sensitive function of tube length.

4. Analysis of results

4.1. *General*

For this purpose we refer to figures 9(*a*)–9(*c*), which are a summary of data for flow rates, v_M, compositions and temperatures, for a tube of radius, $r_0 = 0.5$ mm and length $l = 60$ mm. Figures 9(*b*) and 9(*c*) also include compositions, C_L, and temperatures, T_L, according to the phase diagram of figure 1, as they would apply within a quiescent mushy region. Similar data are available for larger and smaller radii. In all cases, the observed flow rates gradually decelerate towards maxima, regime A, decreasing thereafter despite the rising water content and increased buoyancy, regime B.

Qualitatively, the results illustrate a transition from buoyancy-driven flow at the beginning of an experiment to essentially entrainment-limited flow at later stages. Since volume flow in a tube is proportional to r_0^4 and entrainment into a channel of the same width is proportional to r_0 or $\ln r_0$, it is also to be expected that entrainment limitations will arise sooner (smaller d/h) with wider tubes than with narrower tubes, as the results illustrate.

With the detailed data which are available from these experiments it should be possible to analyse these competing contributions in a quantitative manner. To do this, we consider that the experiments were conducted within a closed system in which liquid circulation must be continuous. Thus, the entrained volume flow, Q_E, equals that flowing up a tube, Q_M (from measured flow rates, v_M), and on up to the free surface. At the upper surface, plumes decelerate and solute (water) spreads out across the upper levels, from which liquid is slowly drawn downwards to be re-entrained. The entire circulatory activity arises as a consequence of the phase transformation (solidification) which proceeds at a rate which is determined by that of the removal of latent heat. Although the energy dissipated in convection is trivial by comparison with the latent heat, the consequences are significant in terms of local and long-range transport. Given that each stage in the circulation is continuous, it is necessary to identify the pressures which are available to drive the system.

4.2. *Estimates of pressures and volume flow rates*

Referring to figure 10, it can be seen that the driving force for circulation must come from the total pressure difference, ΔP_T, between two columns of liquid, P_1, at positions removed from chimney-channels and P_2, along the vertical axis of a chimney at $r = 0$. At either position, these pressures are given by $P = \sum \rho g H$, summed from the level of a tube intake at depth d in the mushy region, figure 10, up to the free surface at H, at atmospheric pressure. In either case, since a rising plume warms up to the bulk temperature, the total temperature interval is

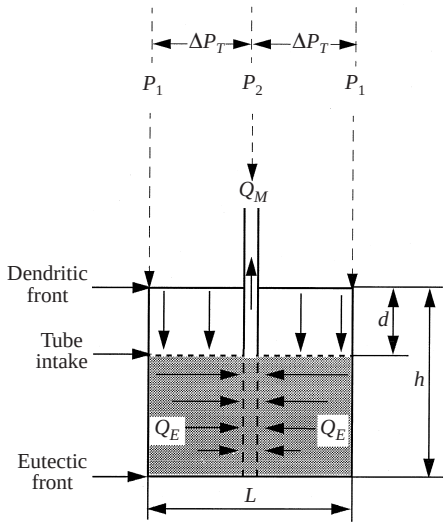

FIGURE 10. Model for entrainment below tube intake and down to eutectic front, radially inwards through a cylinder of radius $\frac{1}{2}L$ and depth $(h-d)$. Volume flow rate for entrainment, Q_E, equals that for flow in tube, Q_M.

almost the same for either column and the difference, ΔP_T, is therefore dominated by solutal considerations. The density at any level is then given by $\rho_L = \rho_0(1-\beta\Delta C)$, where ρ_0 is the liquid density for $C_0 = NH_4Cl$–70%H_2O at the liquidus temperature, 35 °C; β is the solutal expansion coefficient (see table 1) and ΔC the composition difference with respect to C_0. Examples of the estimations of P_1, P_2 and ΔP_T are given in Appendix A. It should be noted that ΔP_T, so obtained, is a small difference between terms which are two orders of magnitude larger, i.e. some 10 Pa instead of 10^3 Pa, and is therefore very sensitive to any errors in assessing the latter. All of these estimated pressures are very small when compared with the atmospheric pressure of 10^5 Pa.

The total presure difference, ΔP_T, is then dissipated into that needed to drive the interdendritic entrainment, ΔP_E, and that needed to overcome viscous drag up a tube and through the bulk liquid up to the free surface, ΔP_M, all volume flow rates being continuous. There will also be a small back pressure attending deceleration at the free surface, ΔP_D, but this is probably negligible (see estimate in Appendix B). Therefore, approximately, $\Delta P_T = \Delta P_E + \Delta P_M$, at any time (equivalent d/h) during an experiment.

The pressure needed to maintain plume flow, ΔP_M, is available from the Poiseuille equation using measured flow rates, v_M. Recollecting that v_M is the maximum velocity in a tube, the volume flow rate is given by:

$$Q_M = \tfrac{1}{2}\pi r_0^2 v_M, \tag{1}$$

where

$$Q_M = \frac{\pi \Delta P_M r_0^4}{8H\eta}, \tag{2}$$

in which H is the total height of the continuous column from a tube intake to the free surface, figure 2. We have already observed that continuity at a tube efflux maintains a constant volume flow rate from within a tube into bulk liquid. An example of such an estimate for ΔP_M is given in Appendix C and the estimated values for ΔP_T and ΔP_M for given tube radius, $r_0 = 0.5$ mm are plotted in figure 11 as a function of tube

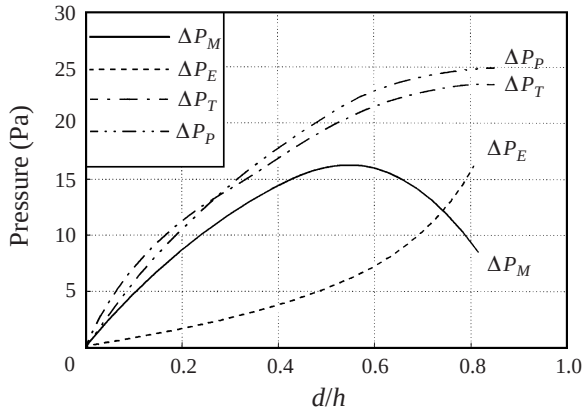

FIGURE 11. Calculated pressure terms *vs.* fractional depth in mushy region, d/h, for tube radius $r_0 = 0.5$ mm. ΔP_M is obtained from measured tube flow rates. $\Delta P_p \approx \Delta P_T$ are the estimated total available pressures to drive circulation and ΔP_E is the pressure needed to effect the necessary entrainment, where $\Delta P_E \approx \Delta P_T - \Delta P_M$.

immersion in the mushy region, d/h. The difference between these is plotted as ΔP_E, being that needed to effect the necessary entrainment.

There is an alternative approach to estimating the total available pressure difference, ΔP_T, which is almost numerically the same as that described previously. It was observed (figure 8) that plume compositions continued to rise beyond maximum flow rates, while streamlined flow continued through regimes B to the point of instability. It was instructive then to take these plume compositions (ΔC, differences with bulk compositions at tube exits) in order to estimate a pressure difference, ΔP_p, which would be available to drive a purely buoyant flow, Q_p, as if there had been no entrainment limitation. ΔP_p is then obtained from the solutal expansion coefficient, β, as previously, and is given by $\Delta\rho g H$, as shown numerically in Appendix D. It will be noticed that the pressure term, ΔP_p, involves the same height as that for viscous drag in the Poiseuille equation (2), so that the volume flow rate is actually independent of height, as experiment confirmed.

It follows that, if there were no limitation to entrainment, $\Delta P_E = 0$, then $\Delta P_T = \Delta P_p$, and indeed, they differ only with estimates of the quiescent density below the growth front, down to a depth d, and the difference is within experimental error, figure 11. Numerical examples of these estimates are given in the Appendices. Inasmuch as the earlier estimates of ΔP_T were sensitive to errors in assessing the larger pressure terms, P_1 and P_2 (figure 10), the above estimates of ΔP_p were preferred, i.e. $\Delta P_p = \Delta P_M + \Delta P_E$ has been used to obtain ΔP_E. It is then possible to consider the entrainment resistance and to use the estimates of ΔP_E for assessments of the permeabilities of the mushy region.

It may be remarked from figure 11 that the stability limit preceding reverse inflow always occurs, for any tube radius, as the ratio of $\Delta P_M : \Delta P_E$ falls below unity (as is also apparent from figure 15). This situation is compatible with earlier comments on figure 7, i.e. the instability leading to reverse inflow occurs soon after the pressure needed to effect entrainment exceeds that required to maintain streamlined tube/plume flow.

4.3. *Entrainment and permeability of the mushy region*

Flow for entrainment takes place downwards into the mushy region, parallel to the primary dendrites and radially inwards into an open channel, normal to the primary,

	$r_0 = 0.4$ mm		$r_0 = 0.5$ mm		$r_0 = 0.75$ mm	
d/h	$K_r(10^{-11})$ m^2	$C_r(10^{-4})$	$K_r(10^{-11})$ m^2	$C_r(10^{-4})$	$K_r(10^{-11})$ m^2	$C_r(10^{-4})$
0.1	4.35	3.2	4.44	3.73	4.6	3.71
0.2	3.85	3.72	3.79	3.75	4.1	3.69
0.3	2.81	2.71	3.6	3.80	3.77	3.88
0.4	2.74	3.11	3.14	3.17		
0.5	2.59	3.08	2.67	3.25		
0.6	2.83	3.36	2.14	2.96		
0.7	2.22	3.24	1.66	2.80		
0.8	2.03	3.41	1.27	2.65		
0.9	1.21	2.72				
	$C_r = 3.17$		$C_r = 3.26$		$C_r = 3.76$	

Weighted average $C_r = 3.30 \pm 20\%\ 10^{-4}$ (weighted according to the ranges of d/h for which streamlined flow occurred.)

TABLE 2. Calculated values for K_r and C_r for 3 tube radii from equations (3) and (4).

branched array. Figure 10 illustrates this pattern schematically, although we recognize that it is a crude simplification of the actual flux pattern. Interdendritic flow parallel to primary dendrites is very much less restricted than that normal to them (Poirier 1987) and the more significant restrictions can be modelled as for a cylinder of radius, $\frac{1}{2}L$ and height $(h - d)$ from figure 10, with flow into the open channel walls of area $2\pi r_0(h - d)$. At the radius, $\frac{1}{2}L$ it is assumed that the liquid is essentially quiescent and we have taken L as a characteristic spacing between naturally occurring channels (and as between those and a constrained tube channel). Observation (e.g. Copley *et al.* 1970; Sample & Hellawell 1982; Sarazin & Hellawell 1988; Tait & Jaupart 1992) shows that this separation, L, is typically of the order $20r_0$, or $\frac{1}{2}L \approx 10r_0$. In expressing radial transport the ratio of $L : 2r_0$ appears as a logarithmic function and is therefore not very sensitive to the assumed value within a range around $\times 10$. In the present experiments, the values of r_0 were predetermined whereas $(h - d)$ decreased continuously throughout an experiment.

From continuity, the measured flow rate, $Q_M = Q_E$, where, for radial flow inwards:

$$Q_E = \frac{2\pi(h - d)K_r \Delta P_E}{\eta \ln (L/2r_0)}, \tag{3}$$

which is the Darcy equation, with K_r as the radial premeability of the mushy region, having dimensions of area. From (3), values of K_r have been calculated, using the available values of Q_M for each tube radius, r_0 at various depths, d, down to the stability limits for streamlined flow.

An example of the calculation of K_r is given in Appendix E and the overall results are listed in table 2. The values so obtained are remarkably consistent, considering the approximations which have been made, and tend to show a small decrease at greater depths in the mushy region, as would be expected.

For the permeability we use the expression:

$$K_r = C_r \lambda_1 \lambda_2 f_L^2 f_s^{-0.75}, \tag{4}$$

which is based on a semiempirical modification of the Poiseuille equation by Poirier

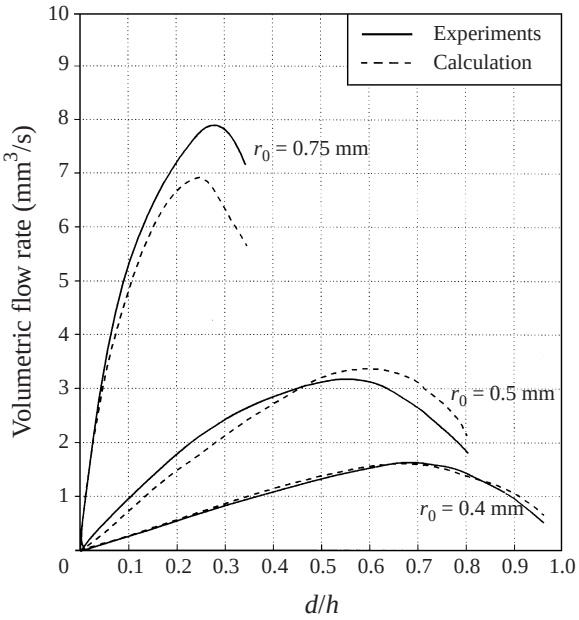

FIGURE 12. Showing volume flow rates from experimental measurments for three tube radii, compared with those calculated for entrainment using average derived permeabilities. Data plotted *vs.* fractional depth of tube intake in the mushy region, d/h.

(1987), following Mehrabian, Keane & Flemings (1970), for flow through interdendritic interstices of primary dendrite spacings, λ_1, and secondary arm spacings, λ_2, as shown in figure 3. The term f_L is the liquid volume fraction, where $f_L = 1 - f_S$, with f_S as the solid fraction and C_r is a constant.

Of these quantities, λ_1 is constant within the duration of an experiment, whereas λ_2 increases with time (therefore depth in the mushy region) by ripening/coarsening (e.g. Marsh & Glicksman 1996) and f_L decreases approximately according to the phase diagram, modified for macrosegregation (e.g. Hellawell *et al.* 1993). It should be understood that these available data for each value of K_r in table 2 are averages taken from the level of a tube intake at depth d, down to the eutectic front, as in the model of figure 10. However, combining these terms in the expression for permeability, equation (4), yields a value for the constant $C_r = 3.3 \times 10^{-4} \pm 20\%$, as in table 2 and Appendix E.

Finally, we take the average calculated value of C_r in the expression for K_r and use it to calculate values for $Q_E = Q_M$, for various tube radii, r_0, and depths of immersion, d. These results are plotted in figure 12, together with the volume flow rates from experiment, Q_M, with which they agree remarkably well, considering the approximations of the model for entrainment. We take this agreement as a satisfactory confirmation of our interpretation of the experimental results, of the identification and interaction between pressure terms, $\Delta P_T = \Delta P_M + \Delta P_E$ and the estimation of their magntiudes.

The derived value of the constant C_r in the expression for permeability, is smaller by nearly an order of magnitude than that given by Poirier (1987). This is probably not a serious discrepancy; the numerical values in the literature are based on regression analysis of limited available experimental data, with confidence ratings around $\pm 50\,\%$. The available published data are for lower liquid fractions ($f_L < 0.66$) than those

applicable in the present system and composition range ($f_L \approx 0.9$). Therefore, the numbers obtained in the present work are essentially without precedent, but are otherwise compatible with the formulation of dendritic dimenions and liquid/solid fractions, as in equation (4). The permeabilities which have been derived are based on *in situ* measurements for radial flow through a square dendritic array, so that the primary spacing, λ_1, is a somewhat ambiguous quantity; thus, if considered diagonally rather than parallel to the array, the value of λ_1 would be effectively smaller, leading to a lower value of the permeability, K_r.

Some comments are needed concerning a permeability estimate for this system by Chen & Chen (1991), which was some two orders of magnitude greater than the present values in table 2. The value quoted by these authors ($\approx 2 \times 10^{-9}\,\mathrm{m}^2$) was based on X-ray absorption data for an NH_4Cl-H_2O mushy region, measured some two days after production when considerable ripening/coarsening would have occurred. The measurements indicated a lower liquid fraction ($f_L \approx 0.65$) than is consistent with composition and mass balance estimates (e.g. Hellawell *et al.* 1993) and the permeability was derived from the Kozeny–Carmen equation (e.g. Michel 1970), using a dimension for primary dendrites which exceeded those typical of the present work by a factor of at least 5. Since the Kozeny–Carman derivation is for the permeability of an assembly of spheres, while a growing dendritic array is highly anisotropic, we have preferred the model of Poirier (1987) and are not able to relate our results to those of Chen & Chen (1991).

In §§ 5 and 6, we use this permeability data to make some assessment of interdendritic entrainment attending the propagation of naturally occurring, unconstrained channel/chimney convection in the same and other systems.

5. Comparisons between constrained and unconstrained situations

As explained in the § 1, this work was motivated by the observation that in experimental laboratory studies of channel formation in widely different material systems, organic, aqueous and metallic, the channel widths are all similar, around 1–2 mm, with spacings around 5–10 mm, although the flow rates involved a range over some two orders of magnitude (Hellawell *et al.* 1993). In an attempt to explain this apparent anomaly we extend the entrainment model developed in the previous constrained analysis to the natural case where channel radii are selected by the system.

The model again involves a cylindrical entrainment volume, but at a level near the growth front rather than deeper in the mushy region; it is somewhat similar to that used by Roberts & Loper (1981) or Sample & Hellawell (1984), as discussed by Worster (1991, 1997). It should be emphasized that we are concerned here only with the quasi-steady-state propagation of channel-chimney plumes and make no attempt to consider preceding events which lead up to the initiation or 'nucleation' of the original eruptions at a growth front. Therefore we are not concerned as to whether channels develop at random local sites (e.g. Sample & Hellawell 1982, 1984) or involve long-range perturbations in the plane of the growth front (e.g. Tait & Jaupart 1992; Worster 1991, 1997).

Inasmuch as we are extending the previous analysis for constrained plume flows, it is first desirable to distinguish the differences in flow patterns between these two situations. Figures 13(*a*) and 13(*b*) are shadowgraphs in the plane of a growth front for constrained and unconstrained examples and figures 14(*a*) and 14(*b*) are corresponding schematic diagrams to show the prevailing flow patterns and catchment volumes which are considered. In either case, the tube or channel exits become surrounded by

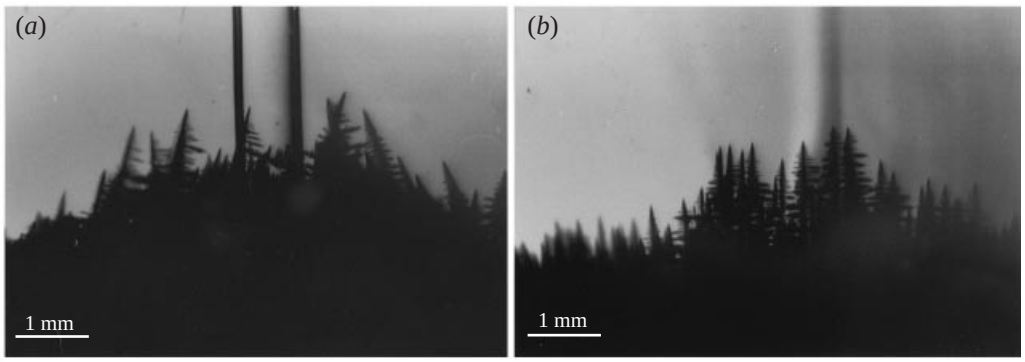

FIGURE 13. Shadowgraphs of channel exits at a dendritic growth front for (*a*) constrained flow within a thin-walled glass tube, and (*b*) at a naturally occurring unconstrained chimney plume. In each case the exits are surrounded by a cone of dendrites produced by local cooling.

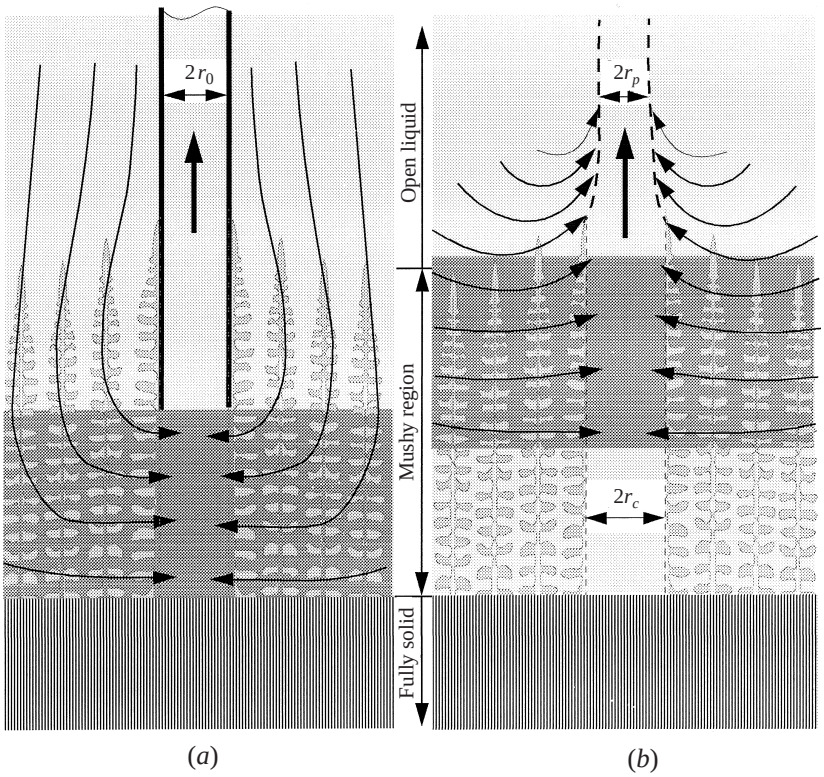

FIGURE 14. Schematic flow patterns corresponding to (*a*) the constrained, and (*b*) the unconstrained cases of figures 1(*a*) and 1(*b*). Relevant radii are as indicated.

a familiar crown of dendrites, rising above the plane of the front; these are caused by local cooling from liquid flowing up from deeper in the mushy region, but the local flow patterns surrounding them are different. In the constrained case, bulk liquid flows slowly down the outer tube walls above the growth front, spreads out laterally and is drawn downwards into the mushy region. Movements of small solid fragments confirm this pattern. In the unconstrained case, the cool effluent at a channel opening

Constrained	Unconstrained
$r = r_0$ constant	r_c/p variable
$Q_{M/P} = Q_E$ continuity	$Q_{M/P} \approx Q_E$
$\Delta P_E + \Delta P_M = \Delta P_T$	$\Delta P_E + \Delta P_{M/P} = \Delta P_T$
d variable	$d = d_0$
ΔC variable (d)	ΔC constant (d_0)
K_r variable (d)	K_r constant (d_0)
$L : r$ constant	$L : r$ constant ($r_p < r_c$)
$H(\Delta P_T)$ constant	$H(\Delta P_T)$ constant
Bulk flow downwards	Bulk flow upwards

TABLE 3. Summary of comparisons between constrained and unconstrained plumes.

draws up the surrounding bulk liquid with it and accelerates as it leaves the channel mouth. Continuity of flow volume requires a corresponding reduction in the cross-section of the solute (water) rich plume as it leaves the mushy region, similar to that at the tube exit of a constrained plume, figure 6. The solute channel in the mushy region below is therefore somewhat wider than the plume which flows upwards towards the free surface. We do not have precise figures for this acceleration and reduction in cross-section; for the constrained case the acceleration was approximately $\times 3$, with a corresponding reduction in width of $\approx 3^{1/2} : 1$, but in the mushy region the channel walls are permeable (in contrast to the tubes) so that the acceleration is smaller, around $\times 2$. Consequently, it is necessary to distinguish the channel radius, r_c, from that of the plume radius, r_p, with $r_c : r_p \approx \sqrt{2} : 1$.

The rising solute plume has a sharp solute profile (witness the step in refractive index) but the velocity profile extends laterally, radially, over a distance comparable with the interchannel separation, $L \approx 20 r_c$ (e.g. Sarazin 1990, Hellawell *et al.* 1993). Consequently, at the plane of the growth front the entrainment flux pattern is quite different to the constrained case, as shown in figure 14(*b*), with a pronounced radial component, actually entering the channel mouth through the dendritic crown, above the plane of the front. Thus, the chilled crown around constrained tubes tends to grow upwards into the cooler downflow whereas around open channel mouths this upward growth is less accentuated.

Below the plane of the growth front, unconstrained entrainment is largely concentrated in the upper levels of the mushy region. Plume concentrations are only 1–2 wt% enriched in water and 5–6 K cooler than the adjacent bulk liquid at channel exists (Hellawell *et al.* 1993). With vertical temperature gradients in the mushy region of about 2.5 K mm^{-1}, this indicates that the average plume composition corresponds to a level of only 2–3 mm below the level of a growth front. Circulation at lower levels in the mushy region is increasingly weak and probably insignificant below a depth, $d_0 < 10$ mm, which is similar to channel spacings. In this respect, the buoyancy pressures in natural unconstrained plumes are much smaller than those in the constrained cases where the concentrations rose to as high as 8 wt% water with respect to the bulk liquid. Table 3 summarizes the above comparisons, the notation is as used previously, except that for the unconstrained case measured *(M)* and plume *(P)* are now the same-as $Q_{M/P}$ and $\Delta P_{M/P}$.

With these differences in mind, we consider then that in principle, the widths of unconstrained channels or plumes can be variable. Observation confirms that plume flow rates fluctuate somewhat, especially with variations in the proximity of adjacent

channel plumes, and residual channel concentrations in solidified metallic samples also show fluctuations (Sarazin 1990), so that only quasi-steady state conditions are maintained at any given time.

Also, it must be remembered that the height of the bulk liquid is slowly decreasing with respect to that of the growth front and the solute concentration is rising as solidification proceeds, so that local fluctuations are superimposed on a gradually changing environment, which tends to retard channel flow activity (e.g. Sarazin & Hellawell 1988). However, with these reservations, we suppose that at any time, a given channel will tend to assume a width which will maintain a balance in continuity between plume volume flow rate, Q_p, and entrainment volume flow, Q_E. Therefore, at any time and location (channel separation) only a given channel radius, r_c, and plume radius, r_p, can satisfy this requirement. We take this as the necessary criterion for selection of channel-plume widths if there is to be an approach to steady-state conditions. We expect that any local fluctuations in plume flow rates will take place more rapidly than commensurate changes in channel widths, which must involve melting or deposition in order to adjust.

6. Analysis for selection of channel/plume widths

From the preceding we seek to express the volume flows for buoyant plumes and entrainment in order to find dimensions for which these are equal. The dimensions involved, figure 14(*b*), are the channel radius, r_c, the plume radius, r_p (where $r_c/r_p \approx \sqrt{2}$), the mean channel spacing, L, and an effective entrainment depth, d_0 which is similar to L. Initially, we consider only the first two of these dimensions to be variables.

The available pressure to drive the circulation, ΔP_T, must arise, as before, from the pressure difference between those exerted by two columns of liquid, at positions approximately midway between channels $\frac{1}{2}L$, pressure P_1 and at a plume core, $r = 0$, pressure P_2 (figure 10). Since the total temperature difference in each column, up to the free surface, is essentially the same, solutal considerations again dominate and $\Delta P_T = \sum(\rho g H)_1 - \sum(\rho g H)_2 = \delta\rho g H$, where $\delta\rho = \rho_0 \beta \Delta C$, and ρ_0 is the initial liquid density at the growth front, β the solutal expansion coefficient and ΔC the plume *vs.* bulk composition difference. These values for the present system and scale are $\rho_0 = 1.08 \times 10^3\,\mathrm{kg\,m^{-3}}$, $\beta = 2.5 \times 10^{-3}\%^{-1}$, $\Delta C < 2\,\mathrm{wt\%}\ H_2O$ and $H \approx 10^{-1}\,\mathrm{m}$, giving $\Delta P_T < 5\,\mathrm{Pa}$.

For plume flow in the open liquid, the volume flow rate, Q_p, from Sarazin (1990) or Hellawell *et al.* (1993) is given by:

$$Q_p = \frac{\pi \Delta P_p r_p^4}{4H\eta}\left[\ln\frac{2r_p}{L} - \frac{1}{2}\right], \tag{5}$$

where $L \approx 20 r_p$ and ΔP_p is that fraction of ΔP_T needed to drive the plume up to the free surface.

For entrainment, radially inwards through a cylindrical volume of radius $\frac{1}{2}\mathrm{L}$ and depth d_0, the volume flow is given as in the previous equation (3), replacing $(h - d)$ by d_0:

$$Q_E = \frac{2\pi d_0 K_r \Delta P_E}{\eta \ln(L/2r_c)}. \tag{6}$$

As previously, we assume that $\Delta P_P + \Delta P_E = \Delta P_T$, but in this case, ΔP_T is so small that estimates of ΔP_P and ΔP_E from the above equations cannot be sufficiently precise to be entirely confident about their numerical values. Substitution of available data,

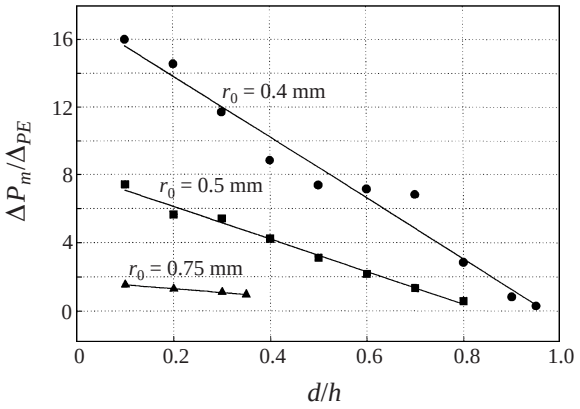

FIGURE 15. Derived pressure ratios for buoyant flow in tubes, ΔP_M, compared with that needed to drive concomitant entrainment, ΔP_E -plotted against fractional depth, d, in mushy region of depth h, for various tube radii, r_0. Data from figure 11.

taking measured maximum plume flow velocities $\approx 10^{-2}\,\mathrm{m\,s^{-1}}$, with $K_r \approx 10^{-10}\,\mathrm{m^2}$ from previous estimates and an assumed value of $r_p = 5 \times 10^{-4}\,\mathrm{m}$, $r_c = \sqrt{2}\,r_p$ and $d_0 = L = 10^{-2}\,\mathrm{m}$, gives $\Delta P_p = 2.8\,\mathrm{Pa}$ and $\Delta P_E \approx 1\,\mathrm{Pa}$. However, while the sum of these numbers is commensurate with that for ΔP_T, the pressure ratio, $\Delta P_p : \Delta P_E$ is itself a variable with the assumed plume or channel radii. Therefore, while the dimensions are all compatible with observations within acceptable ranges, there is an interdependence between the pressure terms and the channel or plume radii (and the ratio between them). Thus, smaller radii match larger pressure ratios and vice versa.

Equivalent information for these relative pressure terms, needed to maintain continuity, is also available from the previous analysis. Thus, for a given tube radius, the pressure needed to effect entrainment rises for greater depths in the mushy region, so that $\Delta P_M/\Delta P_E$ falls progressively with fractional depths, d/h, as shown in figure 15. For the unconstrained model, it has been assumed that the entrainment depth, d_0, is approximately constant, around $10^{-2}\,\mathrm{m}$, or $d/h \approx 0.5$. Thus, in figure 15 at $d/h = 0.5$, the balance ratios rise from $\Delta P_M/\Delta P_E \approx 3$ for a tube of radius $r_0 = 0.5\,\mathrm{mm}$ to ≈ 9 for $r_0 = 0.4\,\mathrm{mm}$ at the same d/h. Here, ΔP_M corresponds to flow in a tube, while ΔP_P is the equivalent for unconstrained plume flow from an open channel.

A convenient way to represent this flexible situation is to assume a given pressure ratio, $\Delta P_M/\Delta P_E$, and to plot the variations of plume flow, Q_p, (equation (5)) and entrainment flow, Q_E (equation (6)) as functions of channel or plume radii (also assuming a given ratio between these, cf. above). In figure 16, Q_p appears as negative quantity or demand, dominated by r_p^4 while Q_E is expressed as a positive available supply, rising with $1/\ln(L/2r_c)$, for a given assumed channel spacing, $L \approx 10^{-2}\,\mathrm{m}$ and $d_0 = 10^{-2}\,\mathrm{m}$. Steady-state continuity then occurs when $Q_E = -Q_P$ at given r_c^* and r_p^*.

If all these quantities or ratios were specified, there would be only single solutions for r_c^* and r_p^*, but in practice, there will be a range of solutions, as indicated by the shading in figure 16. This flexibility is inevitable; channels do not have a close-packed distribution across a growth front and the spacing, L, varies considerably (e.g. Tait & Jaupart 1992; Hellawell *et al.* 1993); the depth, d_0, is imprecise and the ratios, $\Delta P_p : \Delta P_E$ and $r_c : r_p$ can only be approximate. Since $\mathrm{d}Q_E/\mathrm{d}r$ is so much smaller than $-\mathrm{d}Q_P\mathrm{d}r$, there is a wider range of channel widths for a corresponding narrower range of plume widths. We infer from this that channel dimensions will respond relatively slowly to fluctuations in plume flow rates and widths.

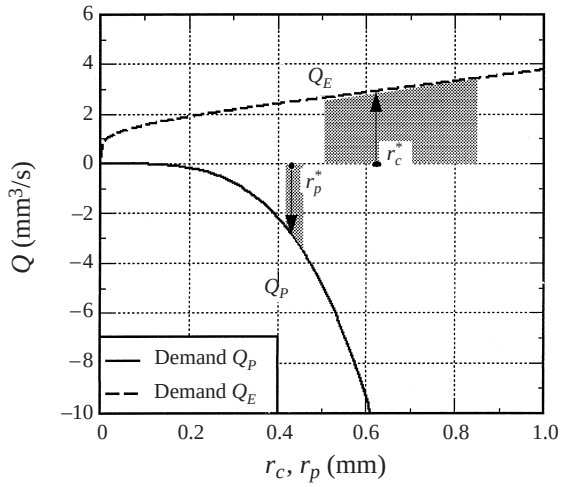

FIGURE 16. Calculated volume flow rates for supply by entrainment, Q_E, *vs.* channel radius and that required by a buoyant plume, Q_p, *vs.* plume radius, r_p (refer to figure 14), assuming a pressure ratio $\Delta P_M : \Delta P_E = 3 : 1$ from figure 15. Steady-state continuity would require that $Q_E = -Q_p$ at r_c^* and r_p^* ($r_c : r_p \approx \sqrt{2} : 1$). Data are for the system NH_4Cl-H_2O, with effective channel depth, $d_0 \approx L$, the mean channel spacing. In practice, there will be a range of solutions for r_p and r_c, as indicated by shading.

Recognizing, then, that steady state is only approximately achieved, it is possible to visualize how the system will respond to fluctuations in plume width (or any other variables, r_c, $\Delta P_p/\Delta P_E$, etc.). We assume that the plume width is the more sensitive to fluctuations: thus, if r_p falls below r_p^*, at $Q_E = -Q_p$, there is an excess of water available in the mushy region, i.e. $Q_E > -Q_p$, so that channel sides will tend to melt and the channel will become wider again. Conversely, if the plume is too wide for steady-state continuity, $Q_E < -Q_p$, the demand for more entrained fluid will draw in more salt-enriched bulk liquid, causing deposition of solid and a reduction in channel width. The situation is, therefore, in a continuous state of fluctuation about preferred steady-state dimensions, and, of course, the relative pressure terms fluctuate accordingly and the effective entrainment depth, d_0, or channel spacing, L, are not well-defined quantities. Nevertheless, given this wide flexibility, the preceding analysis does yield a small range of plume or channel radii which agree closely with observation, in this system, on a laboratory scale. The same approach also yields comparable results for the other material systems, metallic and organic, because the continuity criterion for steady-state selection of radii does not depend upon the absolute magnitudes of the total or separate pressure terms, but only on the relative values of the latter. On the other hand, the magnitude of the pressure terms does directly control those of the volume flow rates, Q_p and Q_E, so that it becomes understandable that the different systems can have similar channel/plume radii but involve widely differing flow rates. This was the apparent anomaly which we sought to resolve.

Thus, in a lead base alloy, within a mould of the same dimensions as that used for the aqueous system, the total pressure difference, $\Delta P_T \approx \delta\rho g H$, with $\delta\rho = \rho_0 \beta \Delta C$, becomes ≈ 100 Pa, compared with 5 Pa for the latter or ≈ 2.5 Pa for the organic system, succinonitrile–ethanol. Variations in the dynamic viscosity coefficients, at least within the ranges involved ($1 - 2.5 \times 10^{-3}$ Pa s), are significant only in that they influence the rate of flow in plumes or during entrainment, but not the dimensions, according to this simple analysis. Rates of flow in plumes of given width, rising through a given height,

should therefore vary relatively with $\Delta P_T/\eta$, so that comparing the above examples, of metallic, aqueous and organic systems, the ratios should be approximately 40 : 5 : 1, which is in good agreement with observations.

We note that, in many respects, the above entrainment analysis is similar to that by Roberts & Loper (1981), as would be expected with an almost identical model. The earlier analysis related to sinking, more dense fluid in a geological context and was in broad general terms, partly limited by lack of numerical data which was not then available. The present analysis is more specific and has the obvious advantage of access to experimentally determined information. In particular, we have addressed the fluctuating interaction between plume flow and channel entrainment, the fact that the radii, r_c and r_p are not equal and that the entrainment depth, d_0, must vary somewhat with the variable channel spacings, L. It should be recognized, however, that the present work concerned rather small-scale laboratory operations and that in a wider geological or oceanographic context (e.g. Huppert & Turner 1980), even metal castings with dimensions up to 1 m would probably be regarded as being of 'laboratory' scale. Nevertheless, the principles should be of general application.

In the crude model for entrainment, the catchment volumes (figure 14) were taken to be cylinders of radii $\frac{1}{2}L$, extending to approximately midway between channels. Nominally, for a given entrainment pressure, ΔP_E, equations (3) and (6) would imply that the volume entrained should rise with decreasing L, according to $1/\ln(L/2r)$, although with ratios around $\times 10$, this is not a sensitive function. However, the opposite occurs, because when two channels are closer than the average separation, competition for supply through overlapping catchment volumes causes the flow activity to wane in one or both channel plumes because there is a deficiency in the supply of less dense, solute-rich liquid. Generally, it is observed that one of these adjacent channels will terminate, i.e. become blocked by deposition of the primary solid. In terms of the total pressure difference between plume columns and that at intermediate positions, the available pressure difference falls, as does that to drive entrainment from one side of a catchment volume.

Formally in our expression for Q_E, equation (6), putting $\mathrm{d}_0 \approx L$, the dependence of Q_E on $d_0(\mathrm{d}Q_E/\mathrm{d}d_0)$ in the numerator, exceeds that of Q_E on L $(\mathrm{d}Q_E/\mathrm{d}\ln L)$ in the denominator, which would explain why the plume activity wanes from one or other channel if two of them grow close to each other. It follows also, that there is a lower limit to the mushy zone depth, h, below which it is not possible to sustain the necessary entrainment to support chimney/plume flow. In the present experimental configuration, this depth, $h > d_0$, was around 12–13 mm.

However, there is evidently an upper limit to d_0, determined not only by the thickness/depth of the mushy region, h, but also by the fact that naturally occurring channels do not remain open throughout the array, but rather become blocked at greater depths by accumulation of dendritic debris which is not ejected into open liquid above (e.g. Hellawell *et al.* 1993, figures 1 and 20). Therefore, if chimney plumes are too widely separated ($L > d_0$), the entrainment volume, Q_E, again decreases or tends towards a maximum value. The preceding analysis therefore offers a qualitative explanation of why an approximate channel spacing should be preferred.

The effects of large changes in viscosity, η, have not been considered here. Formally, both entrainment and plume flow velocities should vary in the same way with viscosity, as in equations (2), (3), (5) and (6), so that there is no obvious reason why the dimensions, r, d_0 or L, should change. However, we note in this connection that Tait & Jaupart (1992) have demonstrated in the NH_4Cl-H_2O system, that if the viscosity is significantly ($\times 50$) increased by the addition of an inert polymer, reduced flow

velocities are also accompanied by increases in channel radii and spacings. It appears that 'slower' equates with 'coarser' and we can offer no explanation for this from our simple analysis of the present experimental work for channel/plume propagation, but the effect may arise during the initial perturbation preceding channel formation.

7. Summary and conclusions

1. Thermosolutal convection has been promoted in thin-walled tubes and measurements have been made for flow rates, composition and temperatures variations within these tubes and in surrounding liquid. The observations illustrate competition between buoyancy-driven convection and the restrictions of fluid entrainment through a mushy region.

2. Entrainment limitations are the more important for wider tubes than for narrower tubes and lead, in all cases, to a breakdown of streamlined flow when the entrained volume falls below a limiting level; this causes instability within a tube and reverse inflow at the upper exit. Subsequent calculations were concerned only with regimes in which streamlined flow was maintained.

3. The results were interpreted in terms of continuity of volume flow rates within a closed system, such that the entrained volume flow, Q_E, must equal the buoyant flow volume, Q_M, up a tube and through supernatant bulk liquid up to the meniscus. The pressure which drives the liquid circulation, ΔP_T, was identified as that between liquid columns at positions remote from and at the core of tube chimney plumes, arising almost entirely from available solutal terms.

4. It was considered that the total available pressure, ΔP_T, was divided between that needed to effect entrainment, ΔP_E, and that needed to overcome viscous drag in an ascending plume, ΔP_M, from measured data. The differences between ΔP_T and ΔP_M provided estimates of the pressure ΔP_E needed to effect entrainment, i.e. to maintain continuity. It was also shown that a hypothetical volume flow, Q_P, based entirely on solutal buoyancy (no entrainment restriction) would involve a necessary pressure, ΔP_P which is almost identical to the total pressure difference ΔP_T.

5. Assuming continuity of flow volumes and using the estimated pressures, ΔP_E, needed to maintain necessary radial entrainment, values were calculated for the permeabilities of the mushy region at different heights normal to the primary dendritic array. These values were then used to back calculate convective flow rates which agreed well with the experimental results from which they were derived.

6. The numerical values of permeabilities in this system, NH_4Cl-H_2O, are expressed as areas, K_r, with confidence limits of about $\pm 20\%$ and provide information which might be usefully employed to model the propagation of natural, unconstrained channel-chimney convection in this system.

7. A simple model has been used to calculate channel-plume width in a solidifying mushy region. The model assumes radial flow through a cylindrical catchment volume into a narrow open channel. While the model is undoubtedly a crude approximation to the actual flux patterns which prevail, the calculations agree well with experimental observations in different material systems under laboratory scale conditions.

8. It is assumed that the preferred width of a channel is that which allows local steady-state continuity to be achieved between entrained liquid and that escaping as a buoyant plume. It is recognized, however, that there are continuous local fluctuations in these volume flow rates so that the channel and plume widths continuously adjust as solidification proceeds. Under laboratory conditions, the available pressures for circulation also change slowly as macrosegregation occurs, so that local short-term

fluctuations are superimposed on these longer-term variations and convective activity gradually declines. The analysis does not explain how channel spacings are preferred except in general qualitative terms.

The present work was conducted as part of a research program concerned with the grain structure of castings, supported by the National Science Foundation, through the Metallurgy Program of the Division of Materials Research, Grant no. DMR 95-21875. The authors wish to acknowledge the assistance of Scott Steube in the development of experimental methods.

Appendix A

Referring to figures 2 or 10, the total pressure available to drive circulation, ΔP_T, should be the difference between the static pressures, P_1 and P_2, respectively, for columns of liquid remote from, and at the core of, a tube plume at $r = 0$. These pressures are then given by $\sum \rho g H$, summed from a tube intake up to the meniscus. Since the total temperature differences over this height are almost the same for both columns, the relevant contributions are almost entirely solutal and are given by the compositions. Therefore, neglecting the vertical temperature gradient, at P_1, the pressure is that from bulk liquid above the growth front over $(H-d)$ and interdendritic liquid down to a depth d; at P_2 the pressure is that for the plume liquid from the base of a tube to the meniscus at height H (this composition does not change with efflux from a tube).

Thus, for the liquid column remote from a plume at $\frac{1}{2}L$, the pressure is given by:

$$P_1 = \int_0^d \rho_L g \mathrm{d}z + \int_d^H \rho_L g \mathrm{d}z.$$

Assuming a linear distribution of solute in the mushy region, the liquid composition, C_L, at any elevation, Z, above the eutectic front can be expressed as:

$$C_L = C_E + \frac{C_B - C_E}{h} Z,$$

where C_E is the eutectic composition and C_B is the mean bulk liquid composition:

$$P_1 = \int_{(h-d)}^h \rho_0 (1 + \beta (C_L - C_0)) g \mathrm{d}z + \int_h^H \rho_0 (1 + \beta (C_B - C_0)) g \mathrm{d}z.$$

At the plume core, $r = 0$, the static pressure for a liquid column of composition C_p is given by:

$$P_2 = \int_0^H \rho_0 (1 + \beta (C_p - C_0)) g \mathrm{d}z.$$

For a tube of radius $r_0 = 0.5\,\mathrm{mm}$, at 1000 s after the start of an experiment, $h = 16.5\,\mathrm{mm}$, $d = 6.6\,\mathrm{mm}$ $(d/h = 0.4)$. Plume composition $C_p = 75.7$ wt%H_2O, bulk composition, $C_B = 70.2$ wt%H_2O, $H = 120\,\mathrm{mm}$, and $H - d = 113.4\,\mathrm{mm}$. This data then yields: $P_1 = 1269$ Pa, $P_2 = 1252$ Pa and $\Delta P_T = 17$ Pa. Such values are plotted in figure 11.

Appendix B

When a liquid plume with attendant bulk flow impinges on the upper free surface, there will be a small back pressure, ΔP_D, attending deceleration. It could be

estimated as:

$$\Delta P_D = \frac{F}{A},$$

where F is the impinging force by the upward flowing plume, acting over an area, A. It is observed that the deceleration takes place over a lateral distance at least equal to that of the wider plume diameter. For a solute plume with attendant bulk flow, this lateral radius, b, of the upward flowing column is at least 5×10^{-3} m, and so the minimum area $A_{min} = \pi b^2$. For a plume with a mean velocity $\bar{v} < 5 \times 10^{-3}\,\mathrm{ms}^{-1}$ and with the above dimension, the deceleration will occur in a time t not less than 1 s, therefore, the force, F, could be found as:

$$F = M\frac{\bar{v}}{t},$$

where M is the mass of the plume column with diameter $2b$ and the height H, so $M = \rho_0 H(\pi b^2)$. By combining all these equations, the back pressure can be estimated as:

$$\Delta P_D = \rho_0 H\frac{\bar{v}}{t} = 1.08 \times 10^3 \times 10^{-1} \times 5 \times 10^{-3} = 0.54\,P_a.$$

This crude estimate is probably an upper limit and may be taken to show that, in this system, the term is not important in the overall pressure balance.

Appendix C

The pressure, ΔP_M, needed to drive tube plume flow is available from the Poiseuille equation (2),

$$Q_M = \frac{\pi \Delta P_M r_0^4}{8H\eta},$$

and Q_M is available from measured maximum flow velocities, v_M, as $Q_M = \frac{1}{2}\pi r_0^2 / v_M$. Thus, with $r_0 = 5 \times 10^{-4}$ m, $v_M = 6 \times 10^{-3}$ ms^{-1}, $H = 10^{-1}$ m and $\eta = 10^{-3}$ Pa s,

$$\Delta P_M = \frac{v_M 4H\eta}{r_0^2} \approx 10\,\mathrm{Pa}.$$

Such values appear in figure 11 for ΔP_M *vs.* fractional immersion, d/h, using experimental velocity measurements from figure 8.

Appendix D

If there were no restrictions to entrainment, buoyant flow would be determined solely by the solutal buoyancy of plume liquid, giving a pressure term, ΔP_p, depending only on the composition difference between plume liquid and the average bulk liquid. Values of ΔP_p are therefore almost the same as those estimated for the total pressure difference, ΔP_T, differing only by density restrictions in the range of the mushy region down to depth, d. At tube exits, the plume liquid had almost reached bulk temperature, so that at that position and up to the meniscus, with a continuous flow volume, $\Delta P_P = \rho_0 \beta \Delta C g H$. For example, with $\Delta C = 5\,\mathrm{wt\%H_2O}$ and $H = 10^{-1}$ m:

$$\Delta P_P = 1080 \times 2.5 \times 10^{-3} \times 5 \times 9.81 \times 10^{-1} = 13.24\,\mathrm{Pa}.$$

The small variations between ΔP_p and ΔP_T are apparent in figure 11 and are almost within the experimental errors involved in measurements of concentrations.

Appendix E

For radial volume flow rate,

$$Q_E = \frac{2\pi(h-d)K_r\Delta P_E}{\eta \ln(L/2r_0)},$$

and continuity requires that $Q_E = Q_M$, the volume flow rate in a tube of radius r_0. The term Q_M is available from measured flow velocities and ΔP_E is available from $\Delta P_T = \Delta P_M + \Delta P_E$, h and d are measured quantities and the ratio $L/2r_0$ is taken as 10, where in this range, ln $(L/2r_0)$ is a relatively insensitive function of the assumed ratio. From the above, values of K_r are obtained for a range of d/h as in table 2.

The semi-empirical expression for K_r is taken from Poirier (1987), as

$$K_r = C_r\lambda_1\lambda_2 f_L^2 f_S^{-0.75},$$

where C_r is a constant. The term λ_1 is effectively a constant ≈ 0.45 mm while λ_2, f_L, and therefore $f_S = 1 - f_L$, vary with time and depth in the mushy region between d and h at the eutectic front. The mean values of λ_2 and f_L for the open channel walls over that distance are calculated as follows.

Side arm spacings, λ_2, coarsen with time behind a growth front (e.g. Glicksman & Voorhees 1984) according to:

$$(\lambda_2^t)^3 - (\lambda_2^0)^3 = Kt,$$

where, for this system, $K \approx 20\ \mu m^3\, s^{-1}$ (Hansen 1995), λ_2^t is the spacing after time t, and λ_2^0 is the initial spacing, $\approx 10\,\mu m$. The liquid fraction, f_L, is assumed to vary linearly from unity at the dendritic front to a minimum at the eutectic front, or, with $f_S = 1 - f_L$,

$$f_L = (1 - f_{SE}) + z/hf_{SE},$$

where f_{SE} is the solid fraction at the eutectic front, calculated from the macroscopic mass balance (Hellawell *et al.* 1993).

Thus, for $r_0 = 0.5$ mm at $d/h = 0.4$, $f_{SE} = 0.125$ (by volume), $(h - d) = 9.9$ mm, giving $K_r = 9.84\ 10^{-8}\ C_r\, m^2$. From the previous expression for Q_E, the same conditions gave a value of $K_r = 3.12 \times 10^{-11}$ m^2, yielding a value for $C_r = 3.2 \times 10^{-4}$. Such are the values listed in table 2 for three tube radii up to the stability limits for streamlined flow.

Appendix F

The thickness of the container or mould was 6 mm, which is a little less than the assumed diameter of a catchment volume, $L \approx 10$ mm. Therefore, the assumption of radial flow was actually modified by the wall effects and reduced by about 28%. In a wider container, without wall effects, the measured flow rates are, in fact, a little greater than those measured in the present experiments, by about 25%. However, this correction does not invalidate the analysis of the results, because all quantities are relative and scale accordingly.

REFERENCES

Bennon, W. D. & Incropera, F. P. 1987 A continuum model for momentum, heat and species transport in binary solid–liquid phase change systems–I. model formulation. *Intl J. Heat Mass Transfer*, **30**, 2161–2170.

Bergman, M. I., Fearn, D. R., Bloxham, J. & Shannon, M. C. 1997 Convection and channel formation in solidifying Pb-Sn alloys. *Metall. Mater. Trans.* A **28**, 859–866.

Chen, C. F. 1995 Experimental study of convection in a mushy layer during directional solidification. *J. Fluid Mech.* **293**, 81–98.

Chen, F. & Chen, C. F. 1991 Experimental study of directional solidification of aqueous ammonium chloride solution. *J. Fluid Mech.* **227**, 567–586.

Copley, S. M., Giamei, A. F., Johnson, S. M. & Hornbecker, M. F. 1970 The origin of freckles in unidirectionally solidified castings. *Metall. Trans.* A **1**, 2193–2204.

Glicksman, M. E. & Voorhees, P. W. 1984 Ostwald ripening and relaxation in dendritic structures. *Metall. Trans.* **15** A, 995–1001.

Hansen, G. C. 1995 Dendritic ripening and fragmentation in 30 wt% NH_4Cl-H_2O. MS thesis, Michigan Technological University, Houghton, MI 49931.

Hellawell, A., Sarazin, J. R. & Steube, R. S. 1993 Channel convection in partly solidified systems. *Phil. Trans. R. Soc. Lond.* A **345**, 507–544.

Huppert, H. E. & Turner, J. S. 1980 Ice blocks melting in a salinity gradient. *J. Fluid Mech.* **100**, 367–384.

Jang, J. & Hellawell, A. 1991 Use of NH_4Cl-H_2O analogue castings to model aspects of continuous casting. Part I, asymmetry in inclined moulds. *J. Ironmaking Steelmaking* **18**, 267–274.

Jorg, O. & Scorer, R. S. 1967 Cold inflow at critical efflux velocities. *Atmos. Environ.* **1**, 645–654.

McDonald, R. J. & Hunt, J. D. 1969 Fluid motion through the partially solid regions of a casting and its importance in understanding A-type segregation. *Trans. Metall. Soc. AIME*, **245**, 1993–1995.

McDonald, R. J. & Hunt, J. D. 1970 Convective fluid motion within the interdendritic liquid of a casting. *Metall. Trans.* A **1**, 1787–1788.

Marsh, S. P. & Glicksman, M. E. 1996 Overview of geometric effects on coarsening of mushy zones. *Metall. Trans.* A **27**, 557–568.

Mehrabian, R., Keane, M. & Flemings, M. C. 1970 Interdendritic fluid flow and macrosegregation; the influence of gravity. *Metall. Trans.* A **1**, 1209–1220.

Michel, S. J. 1970 *Fluid and Particle Mechanics*, ch. 8.5, p. 249. Pergamon.

Moore, J. J. & Shah, N. A. 1983 Mechanisms of formation of 'A' and 'V' segregation in cast steel. *Intl Metall. Rev.* **28**, 338–356.

Poirier, D. R. 1987 Permeability for flow of interdendritic liquid in columnar-dendritic alloys. *Metall. Trans.* B **18**, 245–254.

Roberts, P. H. & Loper, D. E. 1981 Towards a theory of the structure and evolution of a dendrite layer. In *Stellar and Planetary Magnetism.* (ed. A. M. Soward), vol. 2, pp. 329–349.

Sample, A. K. & Hellawell, A. 1982 The effect of mold precession on channel and macrosegregation in ammonium chloride–water analog castings. *Metall. Trans.* B **13**, 495–501.

Sample, A. K. & Hellawell, A. 1984 The mechanism of formation and prevention of channel segregation during alloy solidification. *Metall. Trans.* A **15**, 2163–2173.

Sarazin, J. R. 1990 Buoyancy driven convection and channel segregation during solidification in metallic, aqueous and organic systems, PhD thesis, Michigan Technological University, Houghton, MI 49931.

Sarazin, J. R. & Hellawell, A. 1988 Channel formation in Pb-Sn, Pb-Sb and Pb-Sn-Sb alloy ingots and comparison with the system NH_4Cl-H_2O. *Metall. Trans.* A **19**, 1861–1871.

Scorer, R. S. 1978 *Environmental Aerodynamics,* ch. 8, ch. 10. Ellis Horwood, Chichester, UK.

Steube, R. S. & Hellawell, A. 1993 The use of a transparent aqueous analogue to demonstrate the development of segregation channels during alloy solidification, vertically upwards, *Intl Video J. Engng Res.* **3**, 1–16.

Tait, S. & Jaupart, C. 1992 Compositional convection in a reactive crystalline mush with melt differentiation. *J. Geophys. Res.* **97**, 6735–6756.

Worster, M. G. 1991 Natural convection in a mushy layer. *J. Fluid Mech.* **224**, 335–359.

Worster, M. G. 1997 Convection in mushy layers. *Ann. Rev. Fluid Mech.* **29**, 91–122.